Aerospace Science and Technology 132 (2023) 108064

Contents lists available at ScienceDirect

Aerospace Science and Technology

journal homepage: www.elsevier.com/locate/aescte

Safe navigation of a quadrotor UAV with uncertain dynamics and guaranteed collision avoidance using barrier Lyapunov function ☆

Hamed Habibi [a,*], Ali Safaei [b], Holger Voos [a,c], Mohamed Darouach [d], Jose Luis Sanchez-Lopez [a]

[a] Automation and Robotics Research Group, Interdisciplinary Centre for Security, Reliability and Trust, University of Luxembourg, Luxembourg
[b] Mechanical Engineering Department, McGill University, Montreal, Quebec, Canada
[c] Faculty of Science, Technology and Medicine (FSTM), Department of Engineering, University of Luxembourg, Luxembourg
[d] Université de Lorraine, France

ARTICLE INFO

Article history:
Received 13 June 2022
Received in revised form 14 November 2022
Accepted 8 December 2022
Available online 14 December 2022
Communicated by Tsourdos Antonios

Keywords:
Adaptive model-free control
Barrier Lyapunov function
Motion control
Obstacle avoidance
Preassigned exit time
Quadrotor aerial vehicle

ABSTRACT

In this paper, the safe autonomous motion control of a quadrotor Unmanned Aerial Vehicle (UAV) is considered, in the presence of disturbance, stationary and moving obstacles. In this regard, we directly combine an analytical control design approach, within the backstepping framework, with obstacle avoidance to solve the navigation problem. A Barrier Lyapunov Function (BLF) is incorporated into the translational control to keep the vehicle out of a safety sphere, constructed around the obstacles, while steering it toward a desired position. BLF allows the direct inclusion of the obstacle position in the control design. This is achieved for both cases of known and unknown obstacle velocities. Furthermore, the issue of arbitrary initial conditions is analytically addressed, with a preassigned exit time from the safety sphere. We also consider the case of chance-constrained collision avoidance. The proposed approach leads to a computationally efficient design, since a closed-form of the control is obtained with no need for real-time optimization. More importantly, the analytical stability of closed-loop system is guaranteed. A hierarchical control structure is designed with an adaptive model-free control for unknown attitude dynamics in the presence of disturbances. A number of numerical simulations are performed to evaluate the effectiveness of the proposed approach.

1. Introduction

Quadrotor Unmanned Aerial Vehicles (UAVs) have drawn a great deal of attention in the last decade, due to their outstanding characteristics, such as, low-cost and easy design, versatility, agile maneuverability and Vertical Take-off and Landing (VTOL) capability [1,2]. These make quadrotor UAVs suitable for a large variety of applications, e.g., monitoring, inspection, detection, reconnaissance and mapping [3,4]. However, efficient UAV applications require autonomous operations with many functions performed only with onboard sensors and information processing units such as flight control, perception, localization, navigation, and decision making [5]. Herein, UAV autonomous navigation is a very important topic and hence widely studied in the related literature [6,7]. In general, navigation comprises the task to fly from a start position to the desired position (and orientation) in an often-cluttered environment [8]. For safe navigation, collisions with all stationary as well as moving obstacles in the environment have to be avoided. Often, the way to the desired position is decomposed into a sequence of intermediate waypoints forming a path, leading to the problem of path or trajectory planning and tracking [9]. For instance, in [10], the hybrid Harris hawk optimization (HHO)–grey wolf optimization (GWO) algorithm, to avoid local minima with fast convergence is used. In this paper, we do not consider the planning problem but focus on the basic navigation task of reaching a desired position and orientation from the current position while avoiding obstacles, which might, however, also be applied in path tracking.

Among early solutions to the UAV navigation task, the Artificial Potential Function (APF) approach is a very common one. It constructs a potential field in the workspace with an attractive force towards the goal and repulsive forces caused by the obstacles [7,8,11]. The limitations of the APF approach are the existence

☆ This research was supported by the European Union's Horizon 2020 project Secure and Safe Multi-Robot Systems (SESAME) under the grant agreement no. 101017258.

* Corresponding author.
E-mail addresses: hamed.habibi@uni.lu (H. Habibi), ali.safaei@mail.mcgill.ca (A. Safaei), holger.voos@uni.lu (H. Voos), mohamed.darouach@univ-lorraine.fr (M. Darouach), joseluis.sanchezlopez@uni.lu (J.L. Sanchez-Lopez).

https://doi.org/10.1016/j.ast.2022.108064
1270-9638/

of local minima and the occurrence of an oscillating behavior close to obstacles. Alternatively, the Navigation-Function (NF) method has been introduced [12,13], where the workspace of the UAV is transformed via the navigation transformation. This transformation maps the interior of the workspace to a point world (with a spherical boundary), where the UAV and the obstacles are reduced to points, and the control law is designed as the negative gradient of the NF [13]. The NF-based approach is promising for collision avoidance with static obstacles, while some extensions, tackling moving obstacles, can be found in, e.g., [14]. However, the existing works are mostly based on linearized or simplified models of the UAV dynamics [15,11].

Another way to tackle the navigation task is to consider it as a position control problem with state constraints caused by the obstacles. A very prominent solution to this control problem formulation is Model Predictive Control (MPC) [11]. In MPC the control input is obtained by solving an optimal control problem in a receding horizon. Herein, a dynamic model of the UAV is used to formulate the optimal control problem and to predict the effects of the control input. The advantage of MPC is that nonlinear systems and constraints for the control inputs and the states of the system can efficiently be handled. This makes MPC appropriate for navigation, where the distance to obstacles is considered as a state constraint [16,17]. In [18] a Hammerstein model based MPC controller is designed for real time target tracking of three-axis gimbal system applying flight scenarios of UAV to be robust under external disturbances. However, the consequent real-time optimization imposes a high computational burden [19] and only recent advancements in digital processors for small UAVs allow an onboard implementation of MPC approaches [20]. In addition, the underactuated nature of quadrotor UAVs, instability of the open-loop, coupled translational and attitude dynamics, and wind disturbances, deteriorate the performance of these controllers [21]. Because of the complex computation, most approaches assume a linear UAV model leading to failure when the UAV moves away from operational points for which the model is linearized or performs aggressive maneuvers [22]. Moreover, most of the MPC approaches lack a mathematical stability proof [23].

Other designs for position controllers for UAVs follow a more analytical approach, however, they do not include simultaneous obstacle avoidance since consideration of state constraints is difficult. In [24] a hierarchical control architecture is proposed within a backstepping framework. In [25,26] a robust control design is proposed, taking into account the disturbance on the translational dynamics. In [27,28] fractional-order PI control is designed for attitude regulation. In [1] a neural network-based fault-tolerant control scheme is designed for attitude stabilization in the presence of disturbances. In [29] an adaptive cooperative control scheme for networked UAVs is designed using fractional order PID and recurrent neural networks. In [30] metaheuristic optimization algorithm is proposed based on swarm intelligence and Harris Hawks optimization, to estimate the parameters of the PID control algorithm for UAV. Antiwindup control design is proposed in [31] to deal with saturation and computational efficiency. In [32] a nested structure with feedback linearization technique is proposed to be implemented in an embedded micro-controller. In these works, the UAV attitude dynamics are usually assumed to be known which might be a restrictive assumption in practice. This is the case, especially, when the inertia matrix is not precisely known [6,33]. Therefore, it is desirable to have the controller scheme developed for unknown attitude dynamics. Furthermore, the stability of the closed-loop system is to be analytically guaranteed. Moreover, in all these works it is assumed that the obstacle avoidance is already foreseen in the desired trajectory, constructed in the planning step. However, for moving obstacles, the desired trajectory requires to be replanned iteratively, given the new obstacle information, which further increases the real-time computational burden.

Motivated by the aforementioned issues, in this paper we directly combine an analytical control design approach, within the backstepping framework, with obstacle avoidance to solve the navigation problem. We design a robust nonlinear position controller and incorporate the Barrier Lyapunov Function (BLF) method as in [8], to keep the UAV out of a safety sphere, constructed around each obstacle to ensure safety. From a conceptual point of view, this approach follows the same idea as the NF approach, since the BLF allows a direct inclusion of the obstacles in the control design. This leads to a computationally efficient design compared to, e.g., MPC designs, since a closed-form of the control is obtained with no need for real-time optimization. Also, a low pass filter is incorporated into the design, to resolve the issue of the complexity explosion, in contrast to [41]. More importantly, the analytical stability of closed-loop system is guaranteed. In summary, the novel contributions of this paper compared to related works are as follows:

- Compared to APF and NF methods [12,7,34,13], the collision avoidance is fulfilled for both stationary and moving obstacles. This is achieved for both cases of known and unknown obstacle velocity. The stability of the desired position is analytically proven. Moreover, we treat the problem of uncertainties in the positions of the UAV and the obstacles by formulating a collision chance constraint. This problem is tackled for a user-defined collision avoidance probability, without any online optimization, in contrast to some works, e.g., [35,36].
- In contrast to [8], our BLF approach is applicable to any initial condition without restrictions, even including cases where the UAV starts within a safety sphere of an adjacent obstacle. In this case, a user-defined so-called exit time is assigned by which the UAV flies out of the safety sphere.
- Compared to [8] and many other navigation solutions, we consider a full nonlinear dynamic model of the quadrotor UAV with unknown disturbances and uncertainties in the model parameters. A hierarchical structure is designed with an inner attitude stabilizing control for unknown attitude dynamics in the presence of disturbance, prevailing some works, e.g., [37–40]. For this, we incorporate an Adaptive Model-Free Control (AMFC) for unknown attitude dynamics, to broaden the applicability.

The rest of the paper is organized as follows. In Section 2 the quadrotor UAV model is described and some technical preliminaries are given. In Section 3, we present the overall control design and the main theoretical contributions to achieving the desired objectives. Also, the closed-loop stability is proven. Numerical simulations are discussed in Section 4. Finally, the concluding remarks are given in Section 5.

2. Model description and preliminaries

The quadrotor UAV is maneuvered by regulating the rotor speeds of four identical rotors and propellers. This, in turn, imposes the thrust, perpendicular to the body frame, as well as three rotational torques, along body frame axes. The body frame is represented by b_1, b_2 and b_3 axes, indicating pitch, roll and yaw directions, respectively, as illustrated in Fig. 1.

The rotated angles along the body frame, i.e., Euler angles, are denoted by θ, ϕ and ψ for pitch, roll and yaw angles, respectively. The configuration manifold of UAV in the body frame is a special Euclidean group $\mathrm{SE}(3)$. The thrust f_{p_k} and torque τ_{p_k} of each propeller is proportional to the corresponding rotor speed squared, i.e., $f_{p_k} = k_l \omega_k^2$ and $\tau_{p_k} = k_d \omega_k^2$, for k^{th} rotor speed $\omega_k \in \mathbb{R}_{\geq 0}$, $k \in$

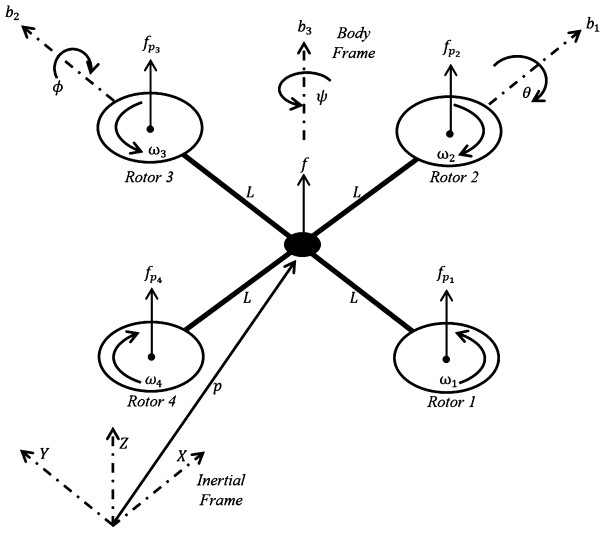

Fig. 1. Quadrotor model.

$\{1, 2, 3, 4\}$, where k_l and k_d are propeller lift and drag coefficients, respectively. The total thrust of $f \in \mathbb{R}_{\geq 0}$ is $f = \sum_{k=1}^{4} f_{p_k}$. It is assumed that the first and the third propellers rotate counterclockwise, and the second and the fourth propellers rotate clockwise. Accordingly, considering the symmetrical structure of a quadrotor UAV, the thrust f and torques vector $\tau = [\tau_{b1}, \tau_{b2}, \tau_{b3}]^T \in \mathbb{R}^3$, in the body frame, can be modeled as

$$\begin{bmatrix} f(t) \\ \tau_{b1}(t) \\ \tau_{b2}(t) \\ \tau_{b3}(t) \end{bmatrix} = \begin{bmatrix} k_l & k_l & k_l & k_l \\ -k_l L & 0 & k_l L & 0 \\ 0 & -k_l L & 0 & k_l L \\ k_d & -k_d & k_d & -k_d \end{bmatrix} \begin{bmatrix} \omega_1^2(t) \\ \omega_2^2(t) \\ \omega_3^2(t) \\ \omega_4^2(t) \end{bmatrix}, \tag{1}$$

where, L is the distance of the rotor center to the UAV center of gravity. As the square matrix in (1) is nonsingular, then by designing f and τ, the values of ω_k can be uniquely computed. The kinematics of the quadrotor UAV is obtained as

$$\dot{p}(t) = v(t), \tag{2a}$$

$$\dot{v}(t) = \frac{1}{M}\left(R(t)F(t) - K_d v(t) - MF_g + f_d(t)\right), \tag{2b}$$

$$\dot{\Phi}(t) = R_q^{-1}(t)\omega(t), \tag{2c}$$

$$\dot{\omega}(t) = J^{-1}(\tau(t) - K_a\omega(t) - \omega(t) \times J\omega(t) + \tau_d(t)), \tag{2d}$$

where, $p = [x, y, z]^T \in \mathbb{R}^3$ and $v = [v_x, v_y, v_z]^T \in \mathbb{R}^3$ are position and velocity vectors of the center of gravity, respectively, in the inertial frame. $\omega \in \mathbb{R}^3$ is the angular velocity in the body frame. M is the known mass and $J \in \mathbb{R}^{3\times 3}$ is the unknown mass moment inertia matrix. $\Phi = [\theta, \phi, \psi]^T \in \mathbb{R}^3$ is the Euler angle vector and $F = [0, 0, f]^T \in \mathbb{R}^3$, both in the body frame. $F_g = [0, 0, g]^T \in \mathbb{R}^3$ is the vector of gravity force in the inertial frame. K_d and K_a are known coefficients of drag force and torque against the translational and angular motions, respectively. Also, $f_d \in \mathbb{R}^3$ and $\tau_d \in \mathbb{R}^3$ are unknown disturbance force and torque, respectively. The rotation matrices $R \in \mathsf{SE(3)}$ and $R_q \in \mathsf{SE(3)}$ are defined as [6]

$$R(t) = \begin{bmatrix} C_\psi C_\theta & C_\psi S_\theta S_\phi - S_\psi C_\phi & C_\psi S_\theta C_\phi + S_\psi S_\phi \\ S_\psi C_\theta & S_\psi S_\theta S_\phi + C_\psi C_\phi & S_\psi S_\theta C_\phi - C_\psi S_\phi \\ -S_\theta & C_\theta S_\phi & C_\theta C_\phi \end{bmatrix}, \tag{3a}$$

$$R_q(t) = \begin{bmatrix} 1 & 0 & -S_\theta \\ 0 & C_\phi & C_\theta S_\phi \\ 0 & -S_\phi & C_\theta C_\phi \end{bmatrix}, \tag{3b}$$

where, C_α and S_α denote cosine and sine of α, respectively. In (2d), it is obvious that the inertia J is affecting the attitude dynamics. The value of J might be hard to obtain accurately [6]. Accordingly, it is reasonable to assume J is unknown, which in turn, makes the attitude dynamics unknown. For the sake of notation simplicity, we present the translational dynamics, i.e., (2a) and (2b), as

$$\dot{x}_1(t) = x_2(t), \tag{4a}$$

$$\dot{x}_2(t) = au(t) + f_1(x) + f_q(t), \tag{4b}$$

where, $x_1 = p$, $x_2 = v$, $u = RF = [u_1, u_2, u_3]^T \in \mathbb{R}^3$, $a = 1/M$, $f_1(x) = a(-K_d v - MF_g)$, $f_q = af_d$. It should be mentioned that the initial condition vector $\bar{x}(0) = [x_1^T(0), x_2^T(0)]^T$ is arbitrary.

Considering the dynamics (2), in this paper we aim to control the rotor speeds ω_k, $k \in \{1, 2, 3, 4\}$, such that to steer the position p towards the desired position $x_d \in \mathbb{R}^3$, for any initial conditions, while keeping the distance from the i^{th} obstacle position $x_{o,i} \in \mathbb{R}^3$, $i \in \{1, ..., m\}$, greater than the user-defined safety bound $R_i \in \mathbb{R}_+$. m is the number of obstacles. For this, we design u in (4), and accordingly, the desired thrust f and orientation Φ are obtained. Consequently, a stabilizing control is designed for the unknown attitude dynamics, i.e., (2c)- (2d), and the desired torque τ is obtained. Finally, the desired rotor speed ω_k is obtained using (1).

Assumption 1. It is assumed that the desired position x_d is known, fixed and collision free. Also, the UAV's states p, v, ω and Φ are available for control design [2]. Moreover, the perception unit shall be able to provide the information on the obstacle position and velocity [8,42]. Finally, disturbances are bounded, i.e., $\|f_d\| \leq \bar{f}_d$ and $\|\tau_d\| \leq \bar{\tau}_d$, where $\bar{f}_d$ and $\bar{\tau}_d$ are unknown positive constants [6].

Remark 1. The fixed desired position x_d in Assumption 1 stems from this fact that usually a higher-level planner exists that schedules the overall task into some waypoints to be followed [43]. Therefore, the proposed control can be extended to the cases where the desired position is variable, i.e., a sequential set of desired positions. It is assumed that the states can be accurately provided, either by on-board sensors such as GPS and inertial measurement unit [44] plus suitable estimators [45–47], or externally provided in experimental flights via a motion capture system such as Opti Track [43]. We assume that the obstacle states can be measured using on-board exteroceptive sensors such as cameras or LIDAR, and suitable sensor and image processing [8].

Remark 2. In a cluttered environment, the obstacles within the workspace of the UAV are only considered. Moreover, a small safety bound can be selected for distant obstacles, to reduce their effects on the control. Accordingly, within the UAV workspace, a compact set $A_{o,i} := \{x_{o,i} \in \mathbb{R}^3 | \|x_{o,i}\|^2 + \|\dot{x}_{o,i}\|^2 \leq \delta_{o,i}\}$, $i \in \{1, ..., m\}$ is considered with unknown positive constant $\delta_{o,i}$, which will be only used in the stability analysis [8].

The following definition and lemmas are used in the design and stability analysis of the proposed control approach.

Definition 1. [48] $x(t)$ is Uniformly Ultimately Bounded (UUB) if there exists a number $T^*(k, x(t_0))$, with $k > 0$ such that for any compact set Ω and all $x(t_0) \in \Omega$, $x(t) \leq k$, for all $t \geq t_0 + T^*$.

Lemma 1. *[49] For any variable $\gamma \in \mathbb{R}$, if $|\gamma| < 1$, the inequality $\tan(\pi\gamma^2/2)/\pi\gamma^2 \leq \sec^2(\pi\gamma^2/2) \leq \sec^4(\pi\gamma^2/2)$ holds.*

Lemma 2. *[50] A scaling function*

$$\varpi(t, T_s) = \begin{cases} 1 - (1 - \frac{t}{T_s})^3 & t < T_s \\ 1 & t \geq T_s \end{cases}, \tag{5}$$

has the following features.

i) $\varpi(t, T_s)$ *is continuous for all* $t \geq 0$ *as* $\lim_{t \to T_s^-} \varpi(t, T_s) = \lim_{t \to T_s^+} \varpi(t, T_s) = 1$.

ii) $\varpi(t, T_s) \in [0, 1]$ *for all* $t \geq 0$.

iii) It is easy to obtain that

$$\dot{\varpi}(t, T_s) = \begin{cases} \frac{3}{T_s}(1 - \frac{t}{T_s})^2 & t < T_s \\ 0 & t \geq T_s \end{cases}. \tag{6}$$

Therefore, $\varpi(t, T_s)$ *is a strictly increasing function starting from* $\varpi(0, T_s) = 0$ *to* $\varpi(T_s, T_s) = 1$, *for* $0 \leq t < T_s$, *and stays at its maximum* $\varpi(t, T_s) = 1$ *for all* $t \geq T_s$.

Lemma 3. *For any variable* $\chi(t) \in \mathbb{R}$ *and positive constant* κ, *the inequality* $0 \leq |\chi| - \chi^2/\sqrt{\chi^2 + \kappa^2} < \bar{c}\kappa$ *holds, where* $\bar{c} = \sqrt{0.5(5\sqrt{5} - 11)} \approx 0.3$.

Proof. Consider the inequality $\chi^4 \leq \chi^2\kappa^2 + \chi^4$ and take the square root from both sides. Then, after some algebraic manipulations, it proves the left side of the inequality. Also, consider the function $G(\chi) = -|\chi| + \chi^2/\sqrt{\chi^2 + \kappa^2}$, which is continuous function. It can be verified that the global minimum of $G(\chi)$ is $-\bar{c}\kappa$, which occurs at $\chi = \pm\kappa\sqrt{((\sqrt{5} - 1)/2)}$. Therefore, it can be concluded that $-\kappa\bar{c} \leq G(\chi)$, and the right side of the inequality is obtained. □

Lemma 4. *[51] Minkowski's Inequality: Let* $\varepsilon > 0$, $p > 1$ *and* $q > 1$ *be real numbers satisfying* $(p - 1)(q - 1) = 1$. *Then for any vectors* $x, y \in \mathbb{R}^n$, *the inequality* $x^T y \leq \varepsilon^p \|x\|^p/p + \|y\|^q/q\varepsilon^q$ *holds.*

Lemma 5. *[35] Consider a linear chance constraint in the form* $Pr\left(a^T x \leq b\right) \leq \delta$, *where* $x \in \mathbb{R}^n$ *is a random variable with a Gaussian distribution, i.e.,* $x \sim \mathcal{N}(\hat{x}, \Sigma)$, $a \in \mathbb{R}^n$ *and* $b \in \mathbb{R}$ *are constants and* δ *is the level of confidence.* $\hat{x} \in \mathbb{R}^n$ *is the mean value vector and* $\Sigma \in \mathbb{R}^{n \times n}$ *is the covariance matrix. Then,* $Pr(a^T x \leq b)$ *can be transformed into a deterministic constraint as* $Pr\left(a^T x \leq b\right) = 0.5\left(1 + \text{erf}\left(\frac{b - a^T\hat{x}}{\sqrt{2a^T\Sigma a}}\right)\right)$, *where* $\text{erf}(z) = \frac{2}{\sqrt{\pi}}\int_0^z e^{-t^2}dt$ *is the standard error function. Moreover, with confidence level* $\delta \in (0, 0.5)$, *we have* $Pr\left(a^T x \leq b\right) \leq \delta \iff a^T\hat{x} - b \geq \text{erf}^{-1}(1 - 2\delta)\sqrt{2a^T\Sigma a}$.

Hereafter, to simplify the subsequent notation, if there is no confusion, function arguments sometimes are omitted.

3. Main results

To construct the obstacle avoidance motion control, define the vector of relative position between the UAV and the desired position, and the distance to the i^{th} obstacle as,

$$e_1(t) = x_1(t) - x_d, \tag{7a}$$

$$d_i(t) = \|x_1(t) - x_{o,i}(t)\|, \tag{7b}$$

respectively, for $i = 1, \ldots, m$. Moreover, define

$$e_2(t) = x_2(t) - z_2(t), \tag{8a}$$

$$X_2(t) = z_2(t) - \alpha_1(t), \tag{8b}$$

where, $\alpha_1 \in \mathbb{R}^3$ is namely the virtual control vector, designed later, in the sense of the backstepping control design framework. In fact, α_1 is not an actual control, instead, it is used in the design of the actual control. In this manner, it is called a virtual control [52]. Also, $z_2 \in \mathbb{R}^3$ is the state of a low pass filter, designed as

$$\tau_2\dot{z}_2(t) + z_2(t) = \alpha_1(t), \tag{9}$$

with the time constant $0 < \tau_2 < 1$. The low pass filter (9) is used to avoid the differentiation of the virtual control α_1 [37].

Considering the user-defined safety bound R_i around the i^{th} obstacle, we define the distance ratio as

$$\gamma_i(t) = \frac{\eta_i(t)R_i}{d_i(t)}, \tag{10}$$

with

$$\eta_i(t) = \begin{cases} \varpi(t, T_{s,i}) & d_i(0) \leq R_i \\ 1 & d_i(0) > R_i \end{cases}, \tag{11}$$

for some user-defined $T_{s,i} \in \mathbb{R}_{\geq 0}$. Considering (10) and (11), for arbitrary initial position $x_1(0)$ of the UAV, it is easy to show that it is always guaranteed that $\gamma_i(0) \in [0, 1)$.

Remark 3. It is obvious that by incorporation of the scaling function (5), no restrictive assumption on the initial condition is required, which resolves a long lasting issue within the context of BLF control design [50]. In fact, the assumption $d_i(0) > R_i$ is no longer needed and the cases of an initial position inside the sphere are automatically handled.

Remark 4. Considering (11), the following points are worth noting.

i) Consider the case that the UAV is initially outside of the safety bound around i^{th} obstacle, i.e., $d_i(0) > R_i$, we have $\eta_i(t) = 1$ and the distance ratio (10) already satisfies $\gamma_i(0) \in [0, 1)$. Then, by guaranteeing $\gamma_i(t) \in [0, 1)$, this implies that $R_i < d_i(t)$ and the obstacle avoidance is always achieved. Therefore, the initial conditions satisfy the requirement in the context of BLF control design [50].

ii) Consider the case that the initial condition is within the safety bound of the i^{th} obstacle, i.e., $d_i(0) \leq R_i$. Even in this case, $\gamma_i(0) = 0 \in [0, 1)$. Then, $\gamma_i(t) \in [0, 1)$ implies that $\eta_i(t)R_i < d_i(t)$. As $\eta_i(t) = 1$ for $t \geq T_{s,i}$, then regardless of the initial conditions, one can obtain that $d_i(t) > R_i$ for $t \geq T_{s,i}$. Therefore, it can be stated that by guaranteeing $\gamma_i(t) \in [0, 1)$, via the proposed control, there exists a time T_i^*, i.e., $0 < T_i^* \leq T_{s,i}$, by which the UAV exits the safety bound R_i around the obstacle. Moreover, $T_{s,i}$ is an arbitrary preassigned exit time by the designer.

Now, we design u in (4b) and the virtual control α_1 as

$$u = \frac{1}{a}\left(-f_1 - \frac{X_2}{\tau_2} - k_2 e_2 - \frac{1}{c_2}(c_1 e_1 - \Gamma_1) - \frac{\hat{f}_q e_2}{\sqrt{\|e_2\|^2 + \alpha_d^2}}\right), \tag{12a}$$

$$\alpha_1 = -k_1 e_1 + \sum_{i=1}^{m} k_{2,i}\sec^2\left(\frac{\pi}{2}\gamma_i^2\right)(x_1 - x_{o,i}) - \frac{c_1 e_1}{2} + \frac{\Gamma_1}{2} + \Gamma_2, \tag{12b}$$

with

$$\Gamma_0 = \sum_{i=1}^{m} c_{i,o}\left(\Gamma_{0,i} + \frac{\eta_i^2}{d_i^4}\sec^2\left(\frac{\pi}{2}\gamma_i^2\right)(x_1 - x_{o,i})^T \dot{x}_{o,i}\right), \tag{13a}$$

$$\Gamma_{0,i} = \frac{\eta_i \dot{\eta}_i}{d_i^2}\sec^2\left(\frac{\pi}{2}\gamma_i^2\right), \tag{13b}$$

$$\Gamma_1 = \sum_{i=1}^{m} c_{i,o}\Gamma_{1,i}(x_1 - x_{o,i}), \tag{13c}$$

$$\Gamma_{1,i} = \frac{\eta_i^2}{d_i^4}\sec^2\left(\frac{\pi}{2}\gamma_i^2\right), \tag{13d}$$

$$\Gamma_2 = -\frac{c_1 e_1 - \Gamma_1}{\|c_1 e_1 - \Gamma_1\|^2}\left(\Gamma_0 + c_1 e_1^T \sum_{i=1}^{m} k_{2,i}\sec^2\left(\frac{\pi}{2}\gamma_i^2\right)(x_1 - x_{o,i}) + k_1 \Gamma_1^T e_1 + \Gamma_3\right), \tag{13e}$$

$$\Gamma_3 = -\sum_{i=1}^{m}\sum_{\substack{j=1 \\ j\neq i}}^{m} c_{i,o} k_{2,j}\Gamma_{1,i}\sec^2\left(\frac{\pi}{2}\gamma_j^2\right)(x_1 - x_{o,i})^T (x_1 - x_{o,j}), \tag{13f}$$

and the adaptive law

$$\dot{\hat{f}}_q = \frac{c_2\|e_2\|^2}{\sqrt{\|e_2\|^2 + \alpha_d^2}} - k_d \hat{f}_q, \tag{14}$$

with the initial condition $\hat{f}_q(0) \in \mathbb{R}_+$. Also k_1, k_2, $k_{2,i}$, k_d, c_1, c_2, $c_{i,o}$ and α_d are positive design parameters, for $i = 1, \ldots, m$. The main properties of the control (12) are summarized in the following theorem.

Theorem 1. *Consider the UAV translational dynamics (4). Under Assumption 1, design the control u and the virtual control α_1 as (12), with (13), the adaptive law (14) and the low pass filter (9). Then, the following objectives are achieved.*

(i) All the closed-loop signals are bounded.
(ii) The UAV position is always kept out of the safety bound R_i around the i^{th} obstacle for $t \geq 0$ when $d_i(0) > R_i$. For the other obstacles, i.e., $d_i(0) \leq R_i$, there exists a time T_i^*, i.e., $0 < T_i^* \leq T_{s,i}$, by which the UAV exits the safety bound, for the preassigned time $T_{s,i}$ and stays out of it for $t \geq T_i^*$.
(iii) The tracking error e_1 is UUB and can be made relatively small by choosing the design parameters properly.

Proof. Consider the positive definite Lyapunov function

$$V = \sum_{i=1}^{5} V_i, \tag{15}$$

where, $V_1 = c_1 e_1^T e_1/2$, $V_2 = c_2 e_2^T e_2/2$, $V_3 = \sum_{i=1}^{m} c_{i,o} V_{i,o}$, $V_{i,o} = \tan(\pi\gamma_i^2/2)/\pi R_i^2$, $V_4 = X_2^T X_2/2$ and $V_5 = \tilde{f}_q^2/2$, where, $\tilde{f}_q = \hat{f}_q - \bar{f}_q$ and $\bar{f}_q = a\bar{f}_d$ is an unknown positive constant. Note $V_{i,o}$ is positive definite in the compact set $\Omega_{i,o} = \{x_1 \in \mathbb{R}^3 | \gamma_i \in [0, 1)\}$ for any given $x_{o,i}$. Accordingly, by taking (4), (7), (8), (10) and (14) into account, one can obtain that

$$\begin{aligned}\dot{V}_{i,o} =& + \frac{\eta_i \dot{\eta}_i}{d_i^2}\sec^2\left(\frac{\pi}{2}\gamma_i^2\right) + \frac{\eta_i^2}{d_i^4}\sec^2\left(\frac{\pi}{2}\gamma_i^2\right)(x_1 - x_{o,i})^T \dot{x}_{o,i} + \\ & - \frac{\eta_i^2}{d_i^4}\sec^2\left(\frac{\pi}{2}\gamma_i^2\right)(x_1 - x_{o,i})^T x_2 \\ =& - \Gamma_{1,i}(x_1 - x_{o,i})^T x_2 + \Gamma_{0,i}.\end{aligned}$$

Consequently,

$$\dot{V}_1 = c_1 e_1^T x_2, \tag{16a}$$

$$\dot{V}_2 = c_2 e_2^T\left(au + f(x) + f_q(t) + \frac{X_2}{\tau_2}\right), \tag{16b}$$

$$\dot{V}_3 = \Gamma_0 - \Gamma_1^T x_2, \tag{16c}$$

$$\dot{V}_4 = -\frac{X_2^T X_2}{\tau_2} - X_2^T \dot{\alpha}_1, \tag{16d}$$

$$\dot{V}_5 = \tilde{f}_q \frac{c_2\|e_2\|^2}{\sqrt{\|e_2\|^2 + \alpha_d^2}} - k_d \tilde{f}_q \hat{f}_q. \tag{16e}$$

Therefore, by using (12) in (16a)-(16c), it is obtained that

$$\begin{aligned}\dot{V}_1 + \dot{V}_2 + \dot{V}_3 =& - c_1 e_1^T k_1 e_1 - k_2 c_2 e_2^T e_2 + (c_1 e_1 - \Gamma_1)^T X_2 + \\ & - \sum_{i=1}^{m} c_{i,o} k_{2,i}\frac{\eta_i^2}{d_i^2}\sec^4\left(\frac{\pi}{2}\gamma_i^2\right) \\ & - c_2 \hat{f}_q \frac{\|e_2\|^2}{\sqrt{\|e_2\|^2 + \alpha_d^2}} + \\ & + c_2 e_2^T f_q(t) - 0.5(c_1 e_1 - \Gamma_1)^T (c_1 e_1 - \Gamma_1).\end{aligned} \tag{17}$$

Considering Lemmas 1 and 4, it is easy to show that

$$(c_1 e_1 - \Gamma_1)^T X_2 \leq \frac{\|c_1 e_1 - \Gamma_1\|^2}{2} + \frac{\|X_2\|^2}{2}, \tag{18a}$$

$$-c_{i,o} k_{2,i}\frac{\eta_i^2}{d_i^2}\sec^4\left(\frac{\pi}{2}\gamma_i^2\right) \leq -c_{i,o} k_{2,i} V_{i,o}, \tag{18b}$$

$$-k_d \tilde{f}_q \hat{f}_q \leq -\frac{k_d}{2}\tilde{f}_q^2 + \frac{k_d}{2}\bar{f}_q^2. \tag{18c}$$

Since α_1 is a function of $\bar{x} = [x_1^T, x_2^T]^T$, x_d, $\hat{f}_q$ and $x_{o,i}$, $i \in \{1, \ldots, m\}$, it can be shown that

$$\dot{\alpha}_1 = \frac{\partial \alpha_1}{\partial \bar{x}}\dot{\bar{x}} + \frac{\partial \alpha_1}{\partial \hat{f}_q}\dot{\hat{f}}_q + \sum_{i=1}^{m}\frac{\partial \alpha_1}{\partial x_{o,i}}\dot{x}_{o,i}. \tag{19}$$

Considering (19), $\dot{\alpha}_1$ is a continuous function and has a maximum constant value M_1 in the compact set $A_1 \times \prod_{i=1}^{m} A_{o,i}$, where, $A_1 := \{[e_1, e_2, \tilde{f}_q, X_2] | V_1 + V_2 + V_4 + V_5 \leq \delta_1\}$ [37]. So, using Lemma 4, one can obtain

$$-X_2^T \dot{\alpha}_1 \leq \frac{\|X_2\|^2}{2} + \frac{M_1^2}{2}. \tag{20}$$

Using (16d), (16e), (17), (18) and (20), it is easy to show that

$$\begin{aligned}\dot{V} \leq & - c_1 e_1^T k_1 e_1 - k_2 c_2 e_2^T e_2 - \sum_{i=1}^{m} k_{2,i} c_{i,o} V_{i,o} - (\frac{1}{\tau_2} - 1)\|X_2\|^2 \\ & - \frac{k_d}{2}\tilde{f}_q^2 + c_2 \tilde{f}_q \frac{\|e_2\|^2}{\sqrt{\|e_2\|^2 + \alpha_d^2}} - c_2 \hat{f}_q \frac{\|e_2\|^2}{\sqrt{\|e_2\|^2 + \alpha_d^2}} \\ & + c_2 e_2^T f_q(t) + \frac{k_d}{2}\bar{f}_q^2 + \frac{M_1^2}{2}.\end{aligned} \tag{21}$$

Moreover, taking Lemma 3 into account, it is easy to show that

$$c_2\tilde{f}_q\frac{\|e_2\|^2}{\sqrt{\|e_2\|^2+\alpha_d^2}}-c_2\hat{f}_q\frac{\|e_2\|^2}{\sqrt{\|e_2\|^2+\alpha_d^2}}+c_2e_2^Tf_q(t)=$$
$$c_2e_2^Tf_q(t)-c_2\bar{f}_q\frac{\|e_2\|^2}{\sqrt{\|e_2\|^2+\alpha_d^2}}$$
$$\leq c_2\bar{f}_q\left(\|e_2\|-\frac{\|e_2\|^2}{\sqrt{\|e_2\|^2+\alpha_d^2}}\right)\leq\bar{c}c_2\bar{f}_q\alpha_d.$$

Therefore, by considering this, (21) yields

$$\dot{V}\leq-k_1c_1e_1^Te_1-k_2c_2e_2^Te_2-\sum_{i=1}^{m}k_{2,i}c_{i,o}V_{i,o}$$
$$-\left(\frac{1}{\tau_2}-1\right)X_2^TX_2-\frac{k_d}{2}\tilde{f}_q^2+\bar{c}c_2\bar{f}_q\alpha_d+\frac{k_d}{2}\bar{f}_q^2+\frac{M_1^2}{2}. \tag{22}$$

Now, by choosing $0<\tau_2<1$, it is readily shown that

$$\dot{V}\leq-\beta_1V+\beta_2, \tag{23}$$

where, $\beta_1=\min_{i=1,..,m}\{2k_1,2k_2,k_{2,i},2(1/\tau_2-1)\}$ and $\beta_2=\bar{c}c_2\bar{f}_q\alpha_d+k_d\bar{f}_q^2/2+M_1^2/2$, are positive constants. Integration of (23) yields

$$V(t)\leq\frac{\beta_2}{\beta_1}+\left(V(0)-\frac{\beta_2}{\beta_1}\right)e^{-\beta_1t}. \tag{24}$$

From the aforementioned analysis, the objectives *(i)*, *(ii)* and *(iii)* are achieved as follows.

(i) As $exp(-\beta_1t)$ is a positive monotonously decreasing function, (24) yields

$$V(t)\leq\frac{\beta_2}{\beta_1}+V(0). \tag{25}$$

This means $V(t)$ is bounded. Considering (15), this further yields that x_1, e_2, X_2 and $\hat{f}_q$ are bounded. Also, $\gamma_i(t)\in[0,1)$, for $i\in\{1,...,m\}$. Accordingly, $\dot{\hat{f}}_q$, u and α_1 are bounded. Finally, z_2 and x_2 are bounded.

(ii) The boundedness of $V(t)$ yields that $V_{i,o}$ is bounded. Therefore, as $\gamma_i(0)=0\in[0,1)$, it is readily shown that $\gamma_i(t)\in[0,1)$, for $i\in\{1,...,m\}$ and $t\geq0$. Therefore, taking (10) into account, this yields $\eta_i(t)R_i<d_i(t)$. Also, considering (11), for i^{th} obstacle such that $d_i(0)>R_i$, $\eta_i(t)=1$. Accordingly, $R_i(t)<d_i(t)$ for $t\geq0$. On the other hand, for other obstacles, i.e., $d_i(0)\leq R_i$, $\eta_i(t)=1$ for $t\geq T_{s,i}$, then regardless of the initial conditions, in accordance to Remark 4 there exists a time T_i^*, such that $R_i(t)<d_i(t)$ for $t\geq T_i^*$.

(iii) Considering (15) and (24), one can obtain that

$$\|e_1\|<\sqrt{\frac{2}{c_1}\left(\frac{\beta_2}{\beta_1}+\left(V(0)-\frac{\beta_2}{\beta_1}\right)e^{-\beta_1t}\right)}. \tag{26}$$

Therefore, if $V(0)=\beta_2/\beta_1$, then $\|e_1\|<\Delta_1$, where $\Delta_1=\sqrt{2\beta_2/c_1\beta_1}$. Also, for $V(0)<\beta_2/\beta_1$, $\|e_1\|<\Delta_1$ is obtained. On the other hand, if $V(0)>\beta_2/\beta_1$, since $lim_{t\to\infty}exp(-\beta_1t)=0$, there exists T such that for any $t>T$, the tracking error enters $\|e_1\|<\Delta_1$. Considering Definition 1, e_1 is UUB. Moreover, Δ_1 can be made arbitrarily small as c_1 and β_1 are based on the design parameters. □

Remark 5. Consider a positive definite Lyapunov function $V^*=V_1+V_3$, that accounts for steering the UAV position towards x_d and, avoiding the obstacles. It is easy to show that $\dot{V}^*=\Gamma_0+(c_1e_1-\Gamma_1)^Tx_2$, where c_1e_1 and Γ_1 represent the weighted distance to the x_d, and weighted summation of distance from the obstacles. In general, V^* might have some local minima, i.e., $c_1e_1-\Gamma_1=0$, at points of the UAV workspace that are away from the destination point. In these cases, $\dot{V}^*=\Gamma_0$, and $\Gamma_0=0$ if the obstacles are far away. Therefore, the UAV is stuck at so-called local minima and it cannot achieve the objectives. Moreover, since $c_1e_1-\Gamma_1=0\Leftrightarrow\|c_1e_1-\Gamma_1\|=0$, there might be a numerical singularity in control (12) (see Γ_2 in (13e)). The fine tuning of c_1 and $c_{i,o}$ can resolve this issue, as recommended in [8]. To do so, we choose random large value for c_1, such that the UAV is always forced towards x_d. Also, we select random small values for $c_{i,o}$. Furthermore, to avoid the numerical singularity, we borrow a solution inspired by Sliding Mode Control, that is, we add a very small constant $\varepsilon_1\in\mathbb{R}_+$ to $\|c_1e_1-\Gamma_1\|$ in the denominator of Γ_2, such that, $\Gamma_2\approx0$ when $\|c_1e_1-\Gamma_1\|=0$, and the numerical singularity is avoided. In this case, more importantly, in (12), the terms k_1e_1 and k_2e_2 still affect the dynamics and steer away from the local minima [8].

Practically, imposing the safety region around the obstacles as a sphere might be unnecessary and reduce the accessible workspace for the UAV, especially for long and slender obstacles. On the other hand, there might be measurement uncertainties on the positions of the UAV and the obstacles. In this regard, some works, e.g., [36,35], have proposed to impose the smallest ellipsoid enclosing the bounding box around the obstacles with a safety radius around the UAV. Then, the chance of the collision is constrained with a predefined probability. In the following proposition, we study the applicability of the proposed control (12) for the collision avoidance with chance constraints.

Proposition 1. *Consider the UAV translational dynamics (4) with Assumption 1. The UAV and obstacles positions measurements follow the Gaussian distribution as* $x_1\sim\mathcal{N}(\bar{x}_1,\Sigma)$ *and* $x_{i,o}\sim\mathcal{N}(\bar{x}_{i,o},\Sigma_{i,o})$, *respectively, with mean values* $\bar{x}_1\in\mathbb{R}^3$ *and* $\bar{x}_{i,o}\in\mathbb{R}^3$ *and covariance matrices* $\Sigma\in\mathbb{R}^{3\times3}$ *and* $\Sigma_{i,o}\in\mathbb{R}^{3\times3}$, *for* $i\in\{1,...,m\}$. *The collision geometry is represented as a sphere with radius* R_r *around the UAV, and a smallest ellipsoid enclosing the obstacle bounding box parametrized by semi-axis lengths* $a_{i,o}$, $b_{i,o}$, *and* $c_{i,o}$. *Consider* $C_{i,o}=\{x_1|(x_1-x_{i,o})^T\Omega_{i,o}(x_1-x_{i,o})\leq1\}$, $\delta_{i,o}\in(0,0.5)$ *and* $\Omega_{i,o}=diag(\frac{1}{(a_{i,o}+R_r)^2},\frac{1}{(b_{i,o}+R_r)^2},\frac{1}{(c_{i,o}+R_r)^2})$. *Design the control* u *and the virtual control* α_1 *as (12) with* $d_i=\|\bar{x}_1-\bar{x}_{o,i}\|$, $erf=\frac{2}{\sqrt{\pi}}\int_0^te^{-t^2}dt$, $R_i=\|\Omega_{i,o}^{0.5}\|\left(\sqrt{2\lambda_{max}(\tilde{\Sigma})}erf^{-1}(1-2\delta_{i,o})+1\right)$, $\tilde{\Sigma}=\Omega_{i,o}^{0.5T}(\Sigma+\Sigma_{i,o})\Omega_{i,o}^{0.5}$, *(13a)-(13f), the adaptive law (14), the low pass filter (9).* $\lambda_{max}(\tilde{\Sigma})$ *denotes the maximum eigenvalue of the matrix* $\tilde{\Sigma}$. *Then the probability of the collision is constrained as* $Pr\{x_1\notin C_{i,o}\}\geq1-\delta_{i,o}$.

Proof. Considering the chance constraints linearization technique given in Lemma 5, we can approximate $C_{i,o}$ as $\tilde{C}_{i,o}=\left\{x_1\middle|a_{r,o}^T(x_1-x_{i,o})\leq1\right\}$, $a_{r,o}=\frac{\Omega_{i,o}^{0.5}(\bar{x}_1-\bar{x}_{o,i})}{\|\Omega_{i,o}^{0.5}(\bar{x}_1-\bar{x}_{o,i})\|}$ such that $Pr\{x_1\notin C_{i,o}\}=Pr\{x_1\notin\tilde{C}_{i,o}\}$ [35]. Furthermore, this can be represented as

$$\frac{\|\bar{x}_1-\bar{x}_{o,i}\|}{\|\Omega_{i,o}^{0.5}\|}\geq erf^{-1}(1-2\delta_{i,o})\sqrt{2a_{r,o}^T\Omega_{i,o}^{0.5T}(\Sigma+\Sigma_{i,o})\Omega_{i,o}^{0.5}a_{r,o}}+1.$$

This inequality, can be further rewritten as $d_i\geq\|\Omega_{i,o}^{0.5}\|erf^{-1}(1-2\delta_{i,o})\sqrt{2a_{r,o}^T\tilde{\Sigma}a_{r,o}}+\|\Omega_{i,o}^{0.5}\|$, with $d_i=\|\bar{x}_1-\bar{x}_{o,i}\|$ and $\tilde{\Sigma}=\Omega_{i,o}^{0.5T}(\Sigma+\Sigma_{i,o})\Omega_{i,o}^{0.5}$. Moreover, it is easy to show that $\sqrt{2a_{r,o}^T\tilde{\Sigma}a_{r,o}}\leq\sqrt{2\lambda_{max}(\tilde{\Sigma})}$. Therefore, it is proven that by satisfying $d_i>R_i$, where $R_i=\|\Omega_{i,o}^{0.5}\|\left(\sqrt{2\lambda_{max}(\tilde{\Sigma})}erf^{-1}(1-2\delta_{i,o})+1\right)$, then, $Pr\{x_1\notin\tilde{C}_{i,o}\}$

is guaranteed, since $erf^{-1}(1-2\delta_{i,o}) > 0$ for $\delta_{i,o} \in (0, 0.5)$. $d_i > R_i$ is achieved by the proposed controller (12), as proven in Theorem 1. □

In the designed control, it is assumed that the obstacle velocities $\dot{x}_{o,i}$, $i \in \{1, ..., m\}$ are available (see (13a)). However, these velocities might not be always measurable accurately and hence could be unknown. Therefore, it is beneficial to analyze the applicability of the proposed control in that situation. In this regard, it is practical to assume that the obstacle velocities are bounded, i.e., $\|\dot{x}_{o,i}\| \leq \bar{V}_{i,o}$, $i \in \{1, ..., m\}$, according to Remark 2, where $\bar{V}_{i,o} \in \mathbb{R}_+$ is an unknown constant. To this end, the following proposition is given.

Proposition 2. *Consider the UAV translational dynamics (4). Under Assumption 1 and unknown obstacle velocities $\dot{x}_{o,i}$, $i \in \{1, ..., m\}$, bounded as $\|\dot{x}_{o,i}\| \leq \bar{V}_{i,o}$, design the control u and the virtual control α_1 as (12), with (13b)-(13e), the adaptive law (14), the low pass filter (9) and*

$$\Gamma_0 = \sum_{i=1}^{m} c_{i,o}\Gamma_{0,i}, \tag{27a}$$

$$\Gamma_3 = -\sum_{i=1}^{m}\sum_{\substack{j=1\\ j\neq i}}^{m} c_{i,o}k_{2,j}\Gamma_{1,i}\sec^2\left(\frac{\pi}{2}\gamma_j^2\right)(x_1 - x_{o,i})^T(x_1 - x_{o,j}) + \sum_{i=1}^{m}\frac{c_{i,o}^2\Gamma_{1,i}^2\|x_1 - x_{o,i}\|^2}{2}. \tag{27b}$$

Then, the objectives (i)-(iii) in Theorem 1 are achieved with error bound

$$\|e_1\| < \sqrt{\frac{2}{c_1}\left(\frac{\beta_3}{\beta_1} + \left(V(0) - \frac{\beta_3}{\beta_1}\right)e^{-\beta_1 t}\right)}, \tag{28}$$

where, $\beta_3 = \beta_2 + 0.5\sum_{i=1}^{m}\bar{V}_{i,o}^2$ is an unknown positive constant.

Proof. The proof is similar to that of Theorem 1 and therefore omitted here for the sake of brevity. □

Remark 6. In Proposition 2, it is obvious that the obstacle velocities $\dot{x}_{o,i}$, $i \in \{1, ..., m\}$ are not used and the stability of the closed-loop system is proven. However, this might lead to a larger tracking error bound (see β_3). Nevertheless, the obstacle avoidance is achieved, satisfying safety constraint R_i. Indeed, this represents the safety aspect of the proposed control, i.e., even if the obstacle information is not completely known, the safety and obstacle avoidance are not compromised.

Now, based on the designed u in (12a), and considering $u = RF = [u_1, u_2, u_3]^T$ and (3), it is easy to obtain the required thrust f as [6]

$$f = \sqrt{u_1^2 + u_2^2 + u_3^2}. \tag{29}$$

Moreover, for a given yaw angle ψ_d, the desired roll and pitch angles are obtained as [6]

$$\phi_d = sin^{-1}\left(\frac{S_{\psi_d}u_1 - C_{\psi_d}u_2}{f}\right), \tag{30a}$$

$$\theta_d = tan^{-1}\left(\frac{C_{\psi_d}u_1 + S_{\psi_d}u_2}{u_3}\right), \tag{30b}$$

respectively. Now, the torques vector τ is designed to regulate the UAV Euler angles Φ to the desired one, i.e., $\Phi_d = [\theta_d, \phi_d, \psi_d]^T \in \mathbb{R}^3$. For this aim, the difference between the desired Euler angles and the actual values is multiplied by a proportional controller to compute a set of desired rates for the Euler angles, i.e., $\dot{\Phi}_d$. Then, the actual rates of Euler angles are computed by multiplying the inverse of R_q matrix into the measured vector of angular velocities. The difference between the desired and actual rates is considered as a tracking error $e = \dot{\Phi}_d - \dot{\Phi}$, where $\dot{\Phi} = R_q^{-1}\omega$ and ω is measured by the on-board sensors. Then, this error is fed into the AMFC [53]. To this end, the attitude dynamics (2d) can be rewritten as

$$\dot{\omega}(t) = A_0\omega(t) + \tau(t) + G_0, \tag{31}$$

where, $A_0 \in \mathbb{R}^{3\times3}$ is an unknown diagonal system matrix and $G_0 = \left(J^{-1} - I_3\right)\tau - J^{-1}K_a\omega - J^{-1}\omega \times J\omega - J^{-1}\tau_d - A_0\omega \in \mathbb{R}^3$ is a vector of unknown nonlinear functions. Accordingly, it is readily obtained that

$$\ddot{\Phi}(t) = A\dot{\Phi}(t) + \tau(t) + G, \tag{32}$$

where, $A \in \mathbb{R}^{3\times3}$ is a unknown diagonal system matrix and $G = R_q^{-1}(A_0R_q\dot{\Phi} + \tau + G_0 - \frac{dR_q}{dt}\dot{\Phi}) - A\dot{\Phi} - \tau \in \mathbb{R}^3$ is a vector of unknown nonlinear functions. Now, the AMFC is designed using the following theorem.

Theorem 2. *Consider the attitude dynamics (2d), represented as (31). Design the torque τ as in (33) where, $\hat{A}$ is the estimation of A, $\zeta = \int_0^t e dt$, and $\sigma = e + \zeta = [\sigma_1, \sigma_2, \sigma_3]^T \in \mathbb{R}^3$. Also, $Q \in \mathbb{R}^{3\times3}$ is positive definite design matrix, and $\bar{\gamma}_1 \in \mathbb{R}^{3\times3}$ and $\bar{\gamma}_2 \in \mathbb{R}^{3\times3}$ are positive definite learning rate matrices. The positive scalars $\bar{\beta}_1$ and $\bar{\beta}_2$ are user-defined leakage gains of the controller. Moreover, $\hat{v} = [\hat{v}_1, \hat{v}_2, \hat{v}_3]^T \in \mathbb{R}^3$. Then, the closed-loop attitude dynamics is stable, all the signals are bounded and the tracking errors e and ζ are UUB.*

$$\begin{aligned}
\tau &= \ddot{\Phi}_d - \hat{A}\dot{\Phi} - \hat{G} - \zeta + \left(I_3 + 2P^{-1}Q + \hat{A}\right)\sigma - \frac{1}{4}P\sigma,\\
\dot{P} &= 2\hat{A}P - P^2 + 2Q,\\
\dot{\hat{G}} &= -\bar{\gamma}_1 P\sigma - \bar{\beta}_1\bar{\gamma}_1\hat{G},\\
\dot{\hat{v}} &= -\bar{\gamma}_2 P M_\sigma(\dot{\Phi} - \sigma) - \bar{\beta}_2\bar{\gamma}_2\hat{v},\\
\hat{A} &= \begin{bmatrix}\hat{v}_1 & 0 & 0\\ 0 & \hat{v}_2 & 0\\ 0 & 0 & \hat{v}_3\end{bmatrix},\\
M_\sigma &= \begin{bmatrix}\sigma_1 & 0 & 0\\ 0 & \sigma_2 & 0\\ 0 & 0 & \sigma_3\end{bmatrix}.
\end{aligned} \tag{33}$$

Proof. See Theorem 1 in [6]. □

Remark 7. As motivated earlier, the attitude dynamics (2d) might be unknown, due to the presence of unknown J. Accordingly, as in the AMFC approach (33), we have not used the attitude dynamics. More importantly, there is no need for manual fine-tuning of the control parameters, since they are either tuned automatically, or designed based on the instruction given in [53]. Note that in (33) the main controller gain matrix, i.e., $P \in \mathbb{R}^{3\times3}$, is a diagonal positive definite matrix whose elements are updated online by solution of a dynamic Riccati equation [48].

Remark 8. The setpoint for the yaw angle ψ_d is commanded by an entity outside of the position control loop. In a hierarchical approach, this desired orientation could be determined by a path planner. This also defines the heading angle of the UAV (and hence

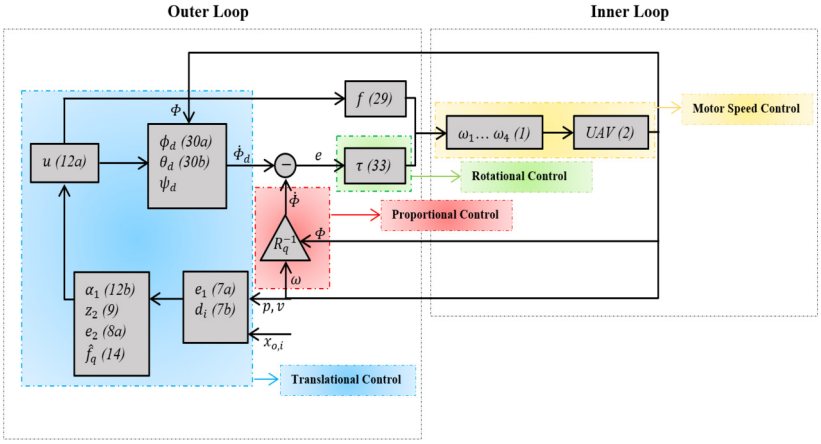

Fig. 2. Overall control structure.

the orientation of some sensors fixed with the body) and does not affect the translational and attitude tracking performance [6].

Remark 9. It should be noted that the dynamics of a conventional quadrotor is underactuated, i.e., there are four control actuators, i.e. ω_k, $k \in \{1, 2, 3, 4\}$, to control six degrees of freedom in a 3D space. Here, this underactuated issue is resolved by utilizing a cascade structure. In this regard, first the translational motion is controlled in an outer loop and the setpoints for roll and pitch angles are determined in (30) along with the external setpoint for yaw angle. Then, in the inner loop, the angular motion is controlled.

Using the thrust f (29) and torque τ (33), the rotor speed ω_k for $k \in \{1, 2, 3, 4\}$ is computed as the inverse of (1). The overall control structure is illustrated in Fig. 2. In this control structure the Euler angles, position and linear and angular velocity vectors of the UAV, and the position of obstacles are fed into the control. The translational tracking error e_1 and distance to the obstacles d_i are computed and (9) and (12b) are solved. Given this, the rates of desired and actual Euler angles are computed, using low level proportional control. The desired Euler angles are computed using the proposed control (12a) and (30). Moreover, (12a) computes the required thrust f. The error between the actual and desired Euler angle rates is fed into (33) to compute the torque τ. Uiing f and τ, the motor speeds are computed using (1) and are commanded to the UAV. The stability of the cascade system is analyzed in the following theorem.

Theorem 3. *Consider the UAV dynamics (2). Under Assumption 1, design the thrust f and torques vector τ as in (29) and (33). Then, the obtained closed-loop system is Input to State Stable (ISS) with respect to disturbances f_d and τ_d, tracking errors e_1, e_2, ξ and e are UUB for bounded disturbances f_d and τ_d and the objectives (i)-(iii) in Theorem 1 are achieved.*

Proof. For given desired Euler angles Φ_d, it is easy to obtain the corresponding rotation matrix $R_d \in \mathrm{SE}(3)$, using (3a). Considering (2), (7a) and (8), it is readily obtained that

$$\dot{e}_1 = v, \tag{34a}$$

$$\dot{e}_2 = \frac{1}{M}\left(R_d F + \left(RR_d^T - I_3\right) R_d F + K_d v - MF_g + f_d\right) - \frac{X_2}{\tau_2}. \tag{34b}$$

Equations (34) along with the attitude dynamics represent a cascade system, in which R_d affects the translation dynamics. The coupling term $RR_d^T - I_3$ represents the attitude tracking error between the desired Euler angles Φ_d and the actual one Φ. In fact, $RR_d^T = I_3$ if and only if $R = R_d^T$, i.e., $\Phi = \Phi_d$. Considering the Rodrigues theorem [54], one can obtain that $\|RR_d^T - I_3\| \leq 2$. Therefore,

$$\|\dot{e}_2\| \leq \|W(e_2)\| + \frac{\|F\|}{M}\left(\|R_d\| + 2\right) + \frac{1}{M}\|f_d\|, \tag{35}$$

where, $W(e_2) = K_d v/M - F_g - X_2/\tau_2$. Moreover, as proven in Theorem 1, the translational dynamics is UUB for given R and bounded f_d, and it is asymptotically stable for $f_d = 0$. Accordingly, for bounded variation Φ_d and f_d the dynamics (35) is ISS according to Definition 2.6 in [55]. Also, the attitude closed-loop dynamics using (33), is UUB for bounded τ_d, and it is asymptotically stable for $\tau_d = 0$. Therefore, according to Theorem 3.1 in [55], the cascade system (34) along with the attitude tracking error dynamics, is ISS with respect to input f_d and τ_d. Therefore, for bounded f_d and τ_d, the tracking errors e_1, e_2 and e are UUB. Also, according to the proof of Theorem 1, objectives *(i)-(iii)* are achieved. □

Remark 10. In the proposed control, one can use the time variable bound $R_i(t)$, to impose time variable safety bounds during the operation. In this case, the proposed approach is still applicable. For this aim, the term $(\Gamma_1 - c_1 e_1)\sum_{i=1}^{m} c_{i,o} W_i / \|c_1 e_1 - \Gamma_1\|^2$, where $W_i = \dot{R}_i \eta_i^2 sec^2(0.5\pi\gamma_i^2)/R_i d_i^2 - 2\dot{R}_i tan(0.5\pi\gamma_i^2)/\pi R_i^3$, is added to α_1 in (12b) and the objectives in Theorem 1 are achieved.

4. Simulation results

In this section, the performance of the proposed scheme is evaluated using simulation examples. The parameters of the UAV dynamic model (2) are as $L = 0.1(m)$, $M = 2(kg)$, $J = 1.24 \times 10^{-3} diag(1, 1, 2)(kgm^2)$, $K_d = 0.01(kg/s)$, $K_a = 0.01(kgm^2/s)$, $k_l = 10^{-5}(kgm)$, $k_d = 10^{-7}(kgm^2)$, $g = 9.81(m/s^2)$, $f_d = sin(t)[0, 0, 1]^T(N)$ and $\tau_d = sin(t)[1, 1, 1]^T(Nm)$ [6]. The initial conditions are as $p(0) = [10, 10, 10]^T(m)$, $\Phi(0) = [0, 0, 0]^T(^\circ)$, $\omega(0) = [0, 0, 0]^T(rad/s)$, $\hat{f}_q(0) = 0.1$ and $z(0) = [0.1, 0.1, 0.1]^T$ with desired position $x_d = [0, 0, 0]^T(m)$. Also, in accordance to Theorem 1 and Remark 7, the control parameters (12) and (33) are selected as $k_1 = 0.1$, $k_2 = 0.001$, $k_{2,i} = 0.001$, $k_d = 5$, $c_1 = 1$, $c_2 = 5$, $c_{i,o} = 3$, $\alpha_d = 0.1$, $\tau_2 = 0.5$, $T_{s,i} = 0.5$, $Q = 0.01 I_3$, $\bar{\gamma}_1 = 10^3 I_3$, $\bar{\gamma}_2 = I_3$, and $\bar{\beta}_1 = \bar{\beta}_2 = 1$. To consider a variety of conditions, we study three different scenarios with moving and stationary obstacles with different safety bounds, and UAV initial velocity including

- *Scenario 1*: Stationary obstacles: $x_{o,1}(0) = [-5, -2, 0]^T$, $x_{o,2}(0) = [-1, -1, -7]^T$, $x_{o,3}(0) = [-1, 4, 0]^T$, $x_{o,4}(0) = [5, 5, 5]^T$,

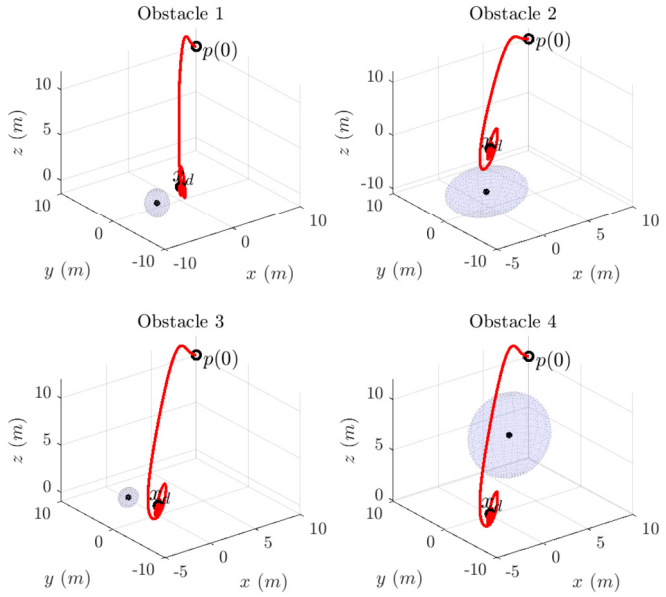

Fig. 3. Trajectory of UAV and obstacles under *Scenario 1*.

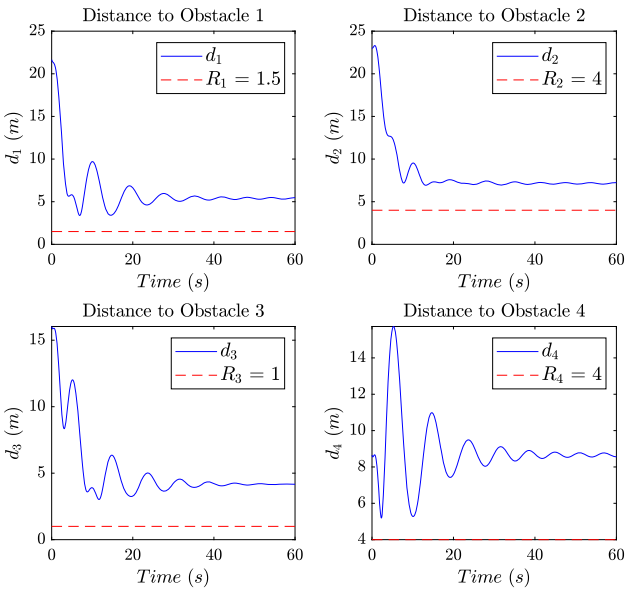

Fig. 4. Distance of UAV and obstacles under *Scenario 1*.

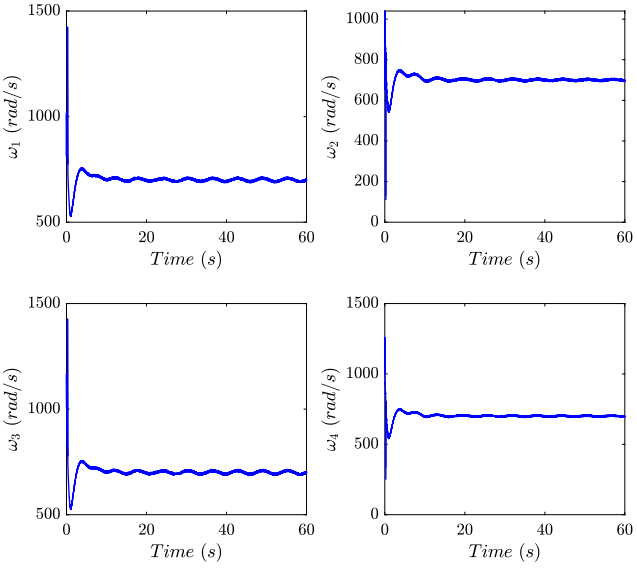

Fig. 5. UAV rotor speeds under *Scenario 1*.

$\dot{x}_{o,i}(t) = [0,0,0]^T$, for $i = 1, ..., 4$, $R_1 = 1.5$, $R_2 = 4$, $R_3 = 1$, $R_4 = 4$ and $v(0) = [-3,0,1]^T$,

- *Scenario 2*: Moving obstacles: $x_{o,1}(0) = [-5,-2,0]^T$, $x_{o,2}(0) = [-1,-1,-7]^T$, $x_{o,3}(0) = [-1,4,0]^T$, $x_{o,4}(0) = [5,5,5]^T$, $\dot{x}_{o,1}(t) = [0.6sin(0.1t), 0.6cos(0.1t), 0]^T$, $\dot{x}_{o,2}(t) = [0.1,-0.1,0.1]^T$, $\dot{x}_{o,3}(t) = [0.4,-0.4,0.2]^T$, $\dot{x}_{o,4}(t) = [0,0,0]^T$, $R_1 = 1.5$, $R_2 = R_4 = 4$, $R_3 = 3$ and $v(0) = [0,0,0]^T$,
- *Scenario 3*: Moving obstacles with initial conditions within the safety sphere: $x_{o,1}(0) = [-4,-2,1]^T$, $x_{o,2}(0) = [-1,-1,-7]^T$, $x_{o,3}(0) = [9,9,9]^T$, $x_{o,4}(0) = [3,4,5]^T$, $\dot{x}_{o,1}(t) = [2sin(0.5t), 2cos(0.5t), 0]^T$, $\dot{x}_{o,2}(t) = [-0.9,-0.9,0.9]^T$, $\dot{x}_{o,3}(t) = [-sin(0.5t), -cos(0.5t), -sin(0.5t)]^T$, $\dot{x}_{o,4}(t) = [-cos(0.5t), cos(0.5t), sin(0.5t)]^T$, $R_1 = 1.5$, $R_2 = 2.95$, $R_3 = 2$, $R_4 = 2.5$, and $v(0) = [-3,0,1]^T$.

In *Scenario 1*, the obstacles are stationary. It is just to verify the stability and convergence of the proposed controller. It is obvious that in *Scenario 2*, we have considered the fourth obstacle exactly on the connecting line $p(0)$ to x_d, which might lead to the local minima issue. Moreover, in *Scenario 3*, the initial distance from the third obstacle is $1.7321(m)$ which lies within the safety bound with the radius $R_3 = 2$. The results are given in Figs. 3-16. In all scenarios, evidently, the desired position is achieved and all the obstacles are avoided, satisfying the given safety bounds (see Figs. 3, 4, 8, 9, 13 and 14). The rotor speeds are shown in Figs. 5, 10 and 15. It is worth noting that the initial increase in the rotor speeds in is due to the effect of gravity. In fact, the UAV starts from $p(0)$ with zero rotor speeds. Then, the designed controller tries to compensate the gravity effect. However, in practice, the UAV starts operating from the ground, i.e., the gravity force is initially canceled by the surface reaction force. Then, the initial sudden increase of the rotor speeds is avoided. As it is observed in Fig. 5, 10 and 15, there are relatively small oscillations in the rotors rotational speed. The root cause is the existence of the external disturbances. We note that the AMFC module is responsible for controlling the attitude dynamics, without having any knowledge neither on the nonlinear dynamics nor on the external disturbances. This is provided in expense of having a UUB convergence with small bounded oscillations around the stable points of the system [6]. The attitude, position error and velocity error with disturbance upper bound estimation are shown in Figs. 6, 11 and 16, which confirm the stability and convergence of the closed-loop system. Also, the UAV velocity vector is illustrated in Figs. 7, 12 and 17. This is more obvious considering the results of *Scenario 1*, i.e., Figs. 3 and 6, where the stability of the desired position is illustrated. In *Scenario 3*, the first obstacle periodically passes close to the desired position. In this situation, the UAV is steered away when this obstacle approaches and then returns to the desired position (see Figs. 13 and 16 (b)). More importantly, the vehicle is initially in the safety sphere around the third obstacle. Then, the UAV exits from this sphere by $T_3^* = 0.27(s) \leq T_{s,3}$, as illustrated in Fig. 14. This is achieved by the scaling function η_3, without any instability or intervention into other safety bounds, considering the other obstacles, which are moving nearby.

Considering these operational scenarios for both moving and stationary obstacles, with different initial conditions of UAV and disturbance effect, it is evident that the closed-loop system is stable and the error of the desired position is UUB as shown in Figs. 3, 8 and 13. Moreover, we have considered the exogenous disturbance on both translational and rotational dynamics, which confirms the robustness of the proposed control. More importantly, in all scenarios the obstacle avoidance is achieved which implies

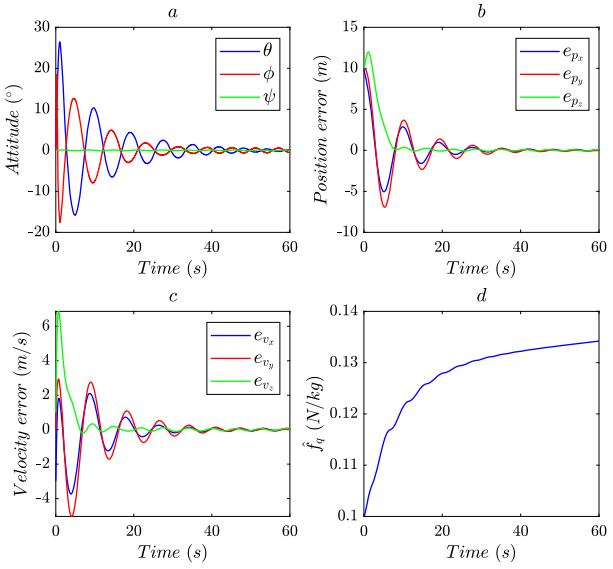

Fig. 6. (a) Attitude, (b) Position error, (c) Velocity error, and (d) Disturbance estimation under *Scenario 1*.

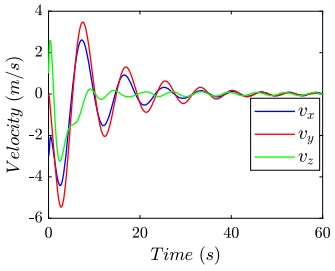

Fig. 7. UAV velocity vector under *Scenario 1*.

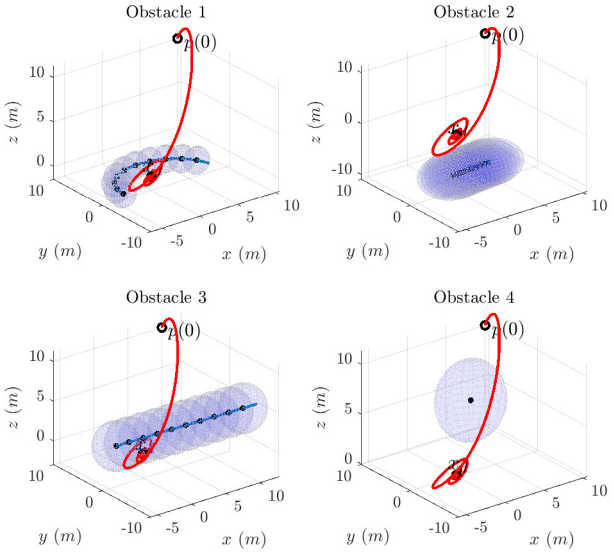

Fig. 8. Trajectory of UAV and obstacles under *Scenario 2*.

the safe autonomous navigation of UAV, as illustrated in Figs. 4, 9 and 14. Furthermore, for arbitrary initial conditions of UAV, even inside of the safety bound, this objective is fulfilled, owning to the incorporation of the scaling function (11) which imposes a user defined exit time. This user defined time can be adjusted considering agility of different UAV models.

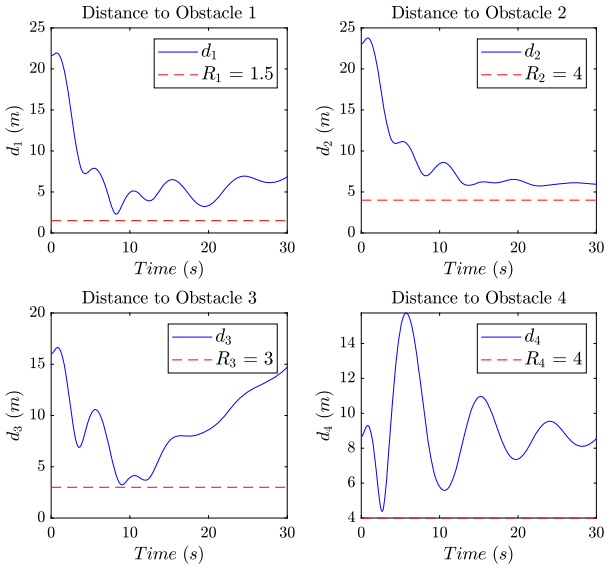

Fig. 9. Distance of UAV and obstacles under *Scenario 2*.

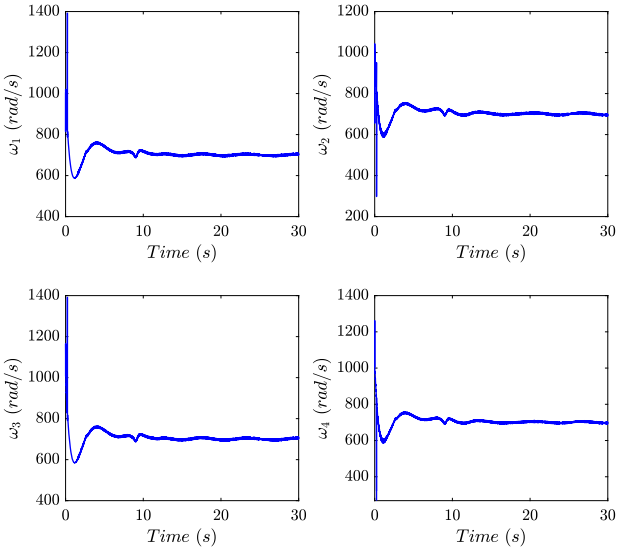

Fig. 10. UAV rotor speeds under *Scenario 2*.

It is worth mentioning that all the results are obtained for the unknown rotational dynamics, which improves applicability of the proposed control for different UAVs. This is due to asymmetrical shape of most of modified UAVs, equipped with different components and sensors. This leads to unknown mass moment inertia and inaccurate geometrical features of UAVs. So, by using the proposed method, the need for accurate estimation of rotational dynamics is relaxed. Finally, it is shown that the actuator efforts, i.e., rotor speeds, are smooth and extremely large control inputs, Figs. 5, 10 and 15, which is a major problem of the nonlinear controls, are avoided. This is, again, due to use of the scaling function, which gradually feeds the large initial error to the control.

Regarding some oscillations around the stable points in Figs. 6, 11 and 16, the main reason is the existence of the disturbance on both translational and rotational dynamics. This is the main feature of UUB stability of the closed-loop system that the tracking error converges to a region around the origin. More importantly, the rotational dynamics is totally unknown which further imposes uncertainty on the control performance. However, the stability is guaranteed and the tracking error margin can be arbitrarily made

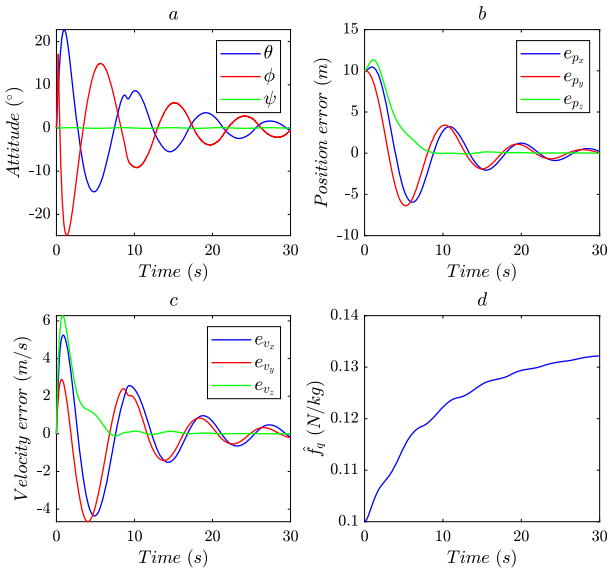

Fig. 11. (a) Attitude, (b) Position error, (c) Velocity error, and (d) Disturbance estimation under *Scenario 2*.

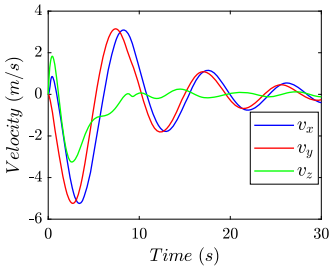

Fig. 12. UAV velocity vector under *Scenario 2*.

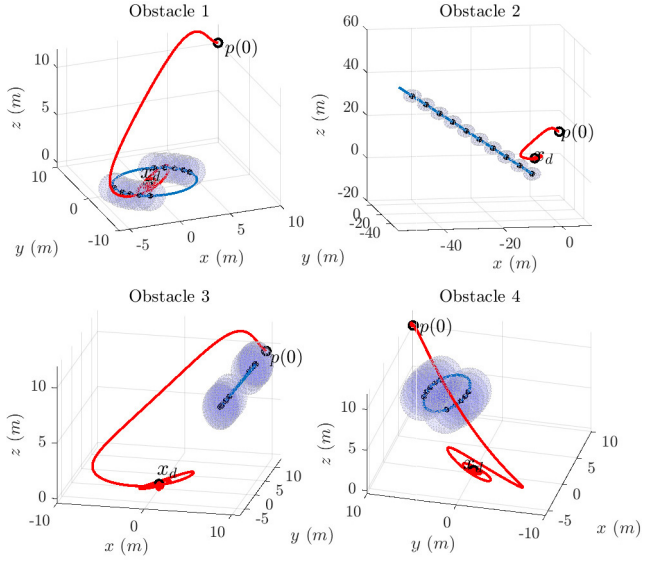

Fig. 13. Trajectory of UAV and obstacles under *Scenario 3*.

small by fine tuning of the control parameters. Also, the spiral motion towards the region around the desired point stems from the exponential convergence of the tracking error as shown in (28), with the rate of β_1. However, the main reason for these oscillations, are the moving obstacles. Considering 8 and 13, it is obvious that there are obstacles moving around the desired points periodically that pushes the UAV away. This motion can be adjusted by selecting small gains c_1 and $c_{i,o}$ in (13e) and (13f), respectively.

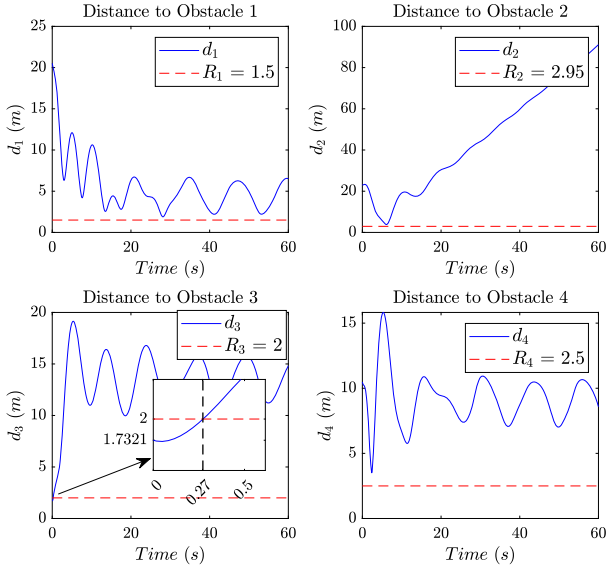

Fig. 14. Distance of UAV and obstacles under *Scenario 3*.

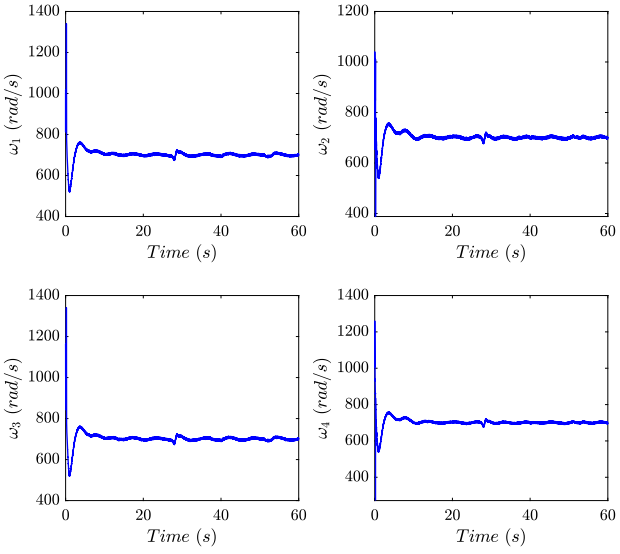

Fig. 15. UAV rotor speeds under *Scenario 3*.

5. Conclusion

In this paper, we considered the problem of safe autonomous motion control of an underactuated quadrotor aerial vehicle. The BLF method was used to design the translational control and to keep the vehicle away from the obstacles, with an assigned safety bound. Also, it was proven that the tracking error is uniformly ultimately bounded. Both cases of known and unknown obstacle velocities were considered. Also, the problem of collision chance constraint, for uncertain vehicle and obstacle positions, was tackled, with no online optimization. The restrictive assumptions on the initial conditions of the vehicle was relaxed by incorporating a scaling function. Moreover, in a hierarchical structure, an adaptive model-free control was designed for unknown attitude dynamics in the presence of disturbance. The numerical simulations were performed and evaluated to show the effectiveness of the proposed approach.

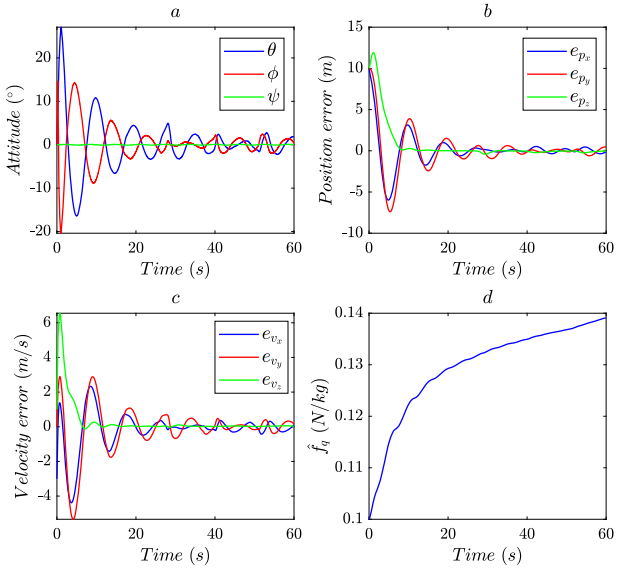

Fig. 16. (a) Attitude, (b) Position error, (c) Velocity error, and (d) Disturbance estimation under *Scenario 3*.

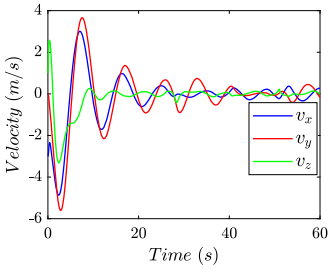

Fig. 17. UAV velocity vector under *Scenario 3*.

Declaration of competing interest

The authors declare that they have no known competing financial interests or personal relationships that could have appeared to influence the work reported in this paper.

Data availability

No data was used for the research described in the article.

References

[1] C. Zhang, M.Z. Dai, J. Wu, B. Xiao, B. Li, M. Wang, Neural-networks and event-based fault-tolerant control for spacecraft attitude stabilization, Aerosp. Sci. Technol. 114 (2021) 106746.
[2] A. Safaei, Adaptive relative velocity estimation algorithm for autonomous mobile robots using the measurements on acceleration and relative distance, Int. J. Adapt. Control Signal Process. 34 (3) (2020) 372–388.
[3] T. Tomic, K. Schmid, P. Lutz, A. Domel, M. Kassecker, E. Mair, I.L. Grixa, F. Ruess, M. Suppa, D. Burschka, Toward a fully autonomous uav: research platform for indoor and outdoor urban search and rescue, IEEE Robot. Autom. Mag. 19 (3) (2012) 46–56.
[4] F. Kendoul, Survey of advances in guidance, navigation, and control of unmanned rotorcraft systems, J. Field Robot. 29 (2) (2012) 315–378.
[5] J.L. Sanchez-Lopez, R.A.S. Fernández, H. Bavle, C. Sampedro, M. Molina, J. Pestana, P. Campoy, Aerostack: an architecture and open-source software framework for aerial robotics, in: International Conference on Unmanned Aircraft Systems (ICUAS), IEEE, 2016, pp. 332–341.
[6] A. Safaei, M.N. Mahyuddin, Optimal model-free control for a generic mimo nonlinear system with application to autonomous mobile robots, Int. J. Adapt. Control Signal Process. 32 (6) (2018) 792–815.
[7] Z. Pan, C. Zhang, Y. Xia, H. Xiong, X. Shao, An improved artificial potential field method for path planning and formation control of the multi-uav systems, IEEE Trans. Circuits Syst. II, Express Briefs 69 (3) (2021) 1129–1133.
[8] E. Restrepo, I. Sarras, A. Loria, J. Marzat, 3d uav navigation with moving-obstacle avoidance using barrier Lyapunov functions, IFAC-PapersOnLine 52 (12) (2019) 49–54.
[9] P. Salaris, M. Cognetti, R. Spica, P.R. Giordano, Online optimal perception-aware trajectory generation, IEEE Trans. Robot. 35 (6) (2019) 1307–1322.
[10] E. Belge, A. Altan, R. Hacıoğlu, Metaheuristic optimization-based path planning and tracking of quadcopter for payload hold-release mission, Electronics 11 (8) (2022) 1208.
[11] B.J. Emran, H. Najjaran, A review of quadrotor: an underactuated mechanical system, Annu. Rev. Control 46 (2018) 165–180.
[12] J. Hong, Y. Kim, H. Bang, Cooperative circular pattern target tracking using navigation function, Aerosp. Sci. Technol. 76 (2018) 105–111.
[13] S.G. Loizou, The navigation transformation, IEEE Trans. Robot. 33 (6) (2017) 1516–1523.
[14] S. Huang, R.S.H. Teo, K.K. Tan, Collision avoidance of multi unmanned aerial vehicles: a review, Annu. Rev. Control 48 (2019) 147–164.
[15] G.P. Roussos, D.V. Dimarogonas, K.J. Kyriakopoulos, 3d navigation and collision avoidance for a non-holonomic vehicle, in: 2008 American Control Conference, IEEE, 2008, pp. 3512–3517.
[16] J. Park, D. Kim, Y. Yoon, H. Kim, K. Yi, Obstacle avoidance of autonomous vehicles based on model predictive control, Proc. Inst. Mech. Eng., Part D, J. Automob. Eng. 223 (12) (2009) 1499–1516.
[17] D. Lee, H. Lim, H.J. Kim, Obstacle avoidance using image-based visual servoing integrated with nonlinear model predictive control, in: 2011 50th IEEE Conference on Decision and Control and European Control Conference, IEEE, 2011, pp. 5689–5694.
[18] A. Altan, R. Hacıoğlu, Model predictive control of three-axis gimbal system mounted on uav for real-time target tracking under external disturbances, Mech. Syst. Signal Process. 138 (2020) 106548.
[19] B. Farzanegan, A.A. Suratgar, M.B. Menhaj, M. Zamani, Distributed optimal control for continuous-time nonaffine nonlinear interconnected systems, Int. J. Control (2021) 1–15.
[20] B. Lindqvist, S.S. Mansouri, A.-a. Agha-mohammadi, G. Nikolakopoulos, Nonlinear mpc for collision avoidance and control of uavs with dynamic obstacles, IEEE Robot. Autom. Lett. 5 (4) (2020) 6001–6008.
[21] A. Abdessameud, A. Tayebi, Global trajectory tracking control of vtol-uavs without linear velocity measurements, Automatica 46 (6) (2010) 1053–1059.
[22] O. Araar, N. Aouf, Full linear control of a quadrotor uav, lq vs h_∞, in: 2014 UKACC International Conference on Control (CONTROL), IEEE, 2014, pp. 133–138.
[23] K. Zhao, Y. Song, C.P. Chen, L. Chen, Control of nonlinear systems under dynamic constraints: a unified barrier function-based approach, Automatica 119 (2020) 109102.
[24] M.-D. Hua, T. Hamel, P. Morin, C. Samson, A control approach for thrust-propelled underactuated vehicles and its application to vtol drones, IEEE Trans. Autom. Control 54 (8) (2009) 1837–1853.
[25] L. Guo, W.-H. Chen, Disturbance attenuation and rejection for systems with nonlinearity via dobc approach, Int. J. Robust Nonlinear Control 15 (3) (2005) 109–125.
[26] X. Wei, L. Guo, Composite disturbance-observer-based control and h∞ control for complex continuous models, Int. J. Robust Nonlinear Control 20 (1) (2010) 106–118.
[27] H. Chao, Y. Luo, L. Di, Y.Q. Chen, Roll-channel fractional order controller design for a small fixed-wing unmanned aerial vehicle, Control Eng. Pract. 18 (7) (2010) 761–772.
[28] J. Han, L. Di, C. Coopmans, Y. Chen, Pitch loop control of a vtol uav using fractional order controller, J. Intell. Robot. Syst. 73 (1) (2014) 187–195.
[29] Z. Yu, Y. Zhang, B. Jiang, C.-Y. Su, J. Fu, Y. Jin, T. Chai, Fractional order pid-based adaptive fault-tolerant cooperative control of networked unmanned aerial vehicles against actuator faults and wind effects with hardware-in-the-loop experimental validation, Control Eng. Pract. 114 (2021) 104861.
[30] A. Altan, Performance of metaheuristic optimization algorithms based on swarm intelligence in attitude and altitude control of unmanned aerial vehicle for path following, in: 2020 4th International Symposium on Multidisciplinary Studies and Innovative Technologies (ISMSIT), IEEE, 2020, pp. 1–6.
[31] P. Ghignoni, D. Invernizzi, M. Lovera, Fixed-dynamics antiwindup design: application to pitch-limited position control of multirotor unmanned aerial vehicles, IEEE Trans. Control Syst. Technol. 29 (6) (2020) 2654–2661.
[32] H. Voos, Nonlinear control of a quadrotor micro-uav using feedback-linearization, in: 2009 IEEE International Conference on Mechatronics, IEEE, 2009, pp. 1–6.
[33] D. Invernizzi, M. Giurato, P. Gattazzo, M. Lovera, Comparison of control methods for trajectory tracking in fully actuated unmanned aerial vehicles, IEEE Trans. Control Syst. Technol. 29 (3) (2020) 1147–1160.
[34] G. Wen, C.P. Chen, Y.-J. Liu, Formation control with obstacle avoidance for a class of stochastic multiagent systems, IEEE Trans. Ind. Electron. 65 (7) (2017) 5847–5855.
[35] H. Zhu, J. Alonso-Mora, Chance-constrained collision avoidance for mavs in dynamic environments, IEEE Robot. Autom. Lett. 4 (2) (2019) 776–783.

[36] M. Castillo-Lopez, P. Ludivig, S.A. Sajadi-Alamdari, J.L. Sanchez-Lopez, M.A. Olivares-Mendez, H. Voos, A real-time approach for chance-constrained motion planning with dynamic obstacles, IEEE Robot. Autom. Lett. 5 (2) (2020) 3620–3625.
[37] X. Shao, J. Liu, H. Cao, C. Shen, H. Wang, Robust dynamic surface trajectory tracking control for a quadrotor uav via extended state observer, Int. J. Robust Nonlinear Control 28 (7) (2018) 2700–2719.
[38] D. Cabecinhas, R. Cunha, C. Silvestre, A nonlinear quadrotor trajectory tracking controller with disturbance rejection, Control Eng. Pract. 26 (2014) 1–10.
[39] W. Dong, G.-Y. Gu, X. Zhu, H. Ding, High-performance trajectory tracking control of a quadrotor with disturbance observer, Sens. Actuators A, Phys. 211 (2014) 67–77.
[40] A. Tayebi, S. McGilvray, Attitude stabilization of a vtol quadrotor aircraft, IEEE Trans. Control Syst. Technol. 14 (3) (2006) 562–571.
[41] G. Dong, L. Cao, D. Yao, H. Li, R. Lu, Adaptive attitude control for multi-muav systems with output dead-zone and actuator fault, IEEE/CAA J. Autom. Sin. 8 (9) (2020) 1567–1575.
[42] W.H. Huang, B.R. Fajen, J.R. Fink, W.H. Warren, Visual navigation and obstacle avoidance using a steering potential function, Robot. Auton. Syst. 54 (4) (2006) 288–299.
[43] J.L. Sanchez-Lopez, M. Castillo-Lopez, M.A. Olivares-Mendez, H. Voos, Trajectory tracking for aerial robots: an optimization-based planning and control approach, J. Intell. Robot. Syst. 100 (2) (2020) 531–574.
[44] J.Q. Cui, S. Lai, X. Dong, B.M. Chen, Autonomous navigation of uav in foliage environment, J. Intell. Robot. Syst. 84 (1) (2016) 259–276.
[45] M. Boutayeb, E. Richard, H. Rafaralahy, H.S. Ali, G. Zaloylo, A simple time-varying observer for speed estimation of uav, IFAC Proc. Vol. 41 (2) (2008) 1760–1765.
[46] G.L. Santosuosso, K. Benzemrane, G. Damm, Nonlinear speed estimation of a gps-free uav, Int. J. Control 84 (11) (2011) 1873–1885.
[47] K. Benzemrane, G.L. Santosuosso, G. Damm, Unmanned aerial vehicle speed estimation via nonlinear adaptive observers, in: 2007 American Control Conference, IEEE, 2007, pp. 985–990.
[48] R.-E. Precup, R.-C. Roman, A. Safaei, Data-driven model-free controllers, 2021.
[49] Z.-L. Tang, K.P. Tee, W. He, Tangent barrier Lyapunov functions for the control of output-constrained nonlinear systems, IFAC Proc. Vol. 46 (20) (2013) 449–455.
[50] Y.-D. Song, S. Zhou, Tracking control of uncertain nonlinear systems with deferred asymmetric time-varying full state constraints, Automatica 98 (2018) 314–322.
[51] M. Sababheh, D. Choi, A complete refinement of Young's inequality, J. Math. Anal. Appl. 440 (1) (2016) 379–393.
[52] T. Madani, A. Benallegue, Control of a quadrotor mini-helicopter via full state backstepping technique, in: Proceedings of the 45th IEEE Conference on Decision and Control, IEEE, 2006, pp. 1515–1520.
[53] A. Safaei, I. Sharf, Adaptive model-free formation-tracking controller and observer for collaborative payload transport by four drones, in: 2021 IEEE International Symposium on Safety, Security, and Rescue Robotics (SSRR), IEEE, 2021, pp. 55–62.
[54] L. Wang, H. Jia, The trajectory tracking problem of quadrotor uav: global stability analysis and control design based on the cascade theory, Asian J. Control 16 (2) (2014) 574–588.
[55] P. Forni, D. Angeli, Input-to-state stability for cascade systems with multiple invariant sets, Syst. Control Lett. 98 (2016) 97–110.